Article

Decay of Root Debris after Harvesting American Ginseng (*Panax quinquefolius*) and Changes in Soil Chemistry and Microbiology

Iván Darío Samur Suárez, Moez Valliani [iD], Tom Hsiang [iD] and Paul H. Goodwin *

School of Environmental Sciences, University of Guelph, 50 Stone Road East, Guelph, ON N1G 2W1, Canada; samurivandario@gmail.com (I.D.S.S.); mvallian@uoguelph.ca (M.V.); thsiang@uoguelph.ca (T.H.)
* Correspondence: pgoodwin@uoguelph.ca

Abstract: Commercial harvesting of American ginseng (*Panax quinquefolius*) results in root debris in the soil, but the rate of decay is unknown. In this study, post-harvest root debris decayed mostly over the fall and winter, with almost no ginseng debris remaining in the soil by late spring of the following year. However, a small number of intact pencil-shaped roots were able to survive after harvest and sprout the following spring without any evidence of root decay. Root rot lesions were observed, which included many associated with the root rot pathogen *Ilyonectria mors-panacis,* with disappearing root rot symptoms observed in the following spring. Ginsenosides in soil were highest just prior to harvest, declining until an increase the following spring. Soil bacterial and fungal populations changed over time after harvest with several peaks in bacterial populations mostly in the fall, but this was less clear for fungal populations, which were dominated by only a few taxa. Harvesting ginseng can leave considerable debris in the soil, impacting its chemistry and microbiota. Ginseng replant disease, where the second crop shows high levels of root rot due to *I. mors-panacis* infection compared to low levels in the first crop, could be related to the decay of post-harvest crop debris, but additional research is needed to demonstrate this.

Keywords: post-harvest decay; soil microbiome; bacteria; fungi; ginsenosides

1. Introduction

While post-harvest crop debris in soil can benefit plants by adding organic matter, it can also lead to harmful effects. For example, crop debris can introduce toxins into soil resulting in allelopathy [1], and allelopathic compounds can also be created via microbial degradation of crop debris [2,3]. Crop debris can also release compounds that can inhibit beneficial soil microorganisms, thus indirectly limiting plant growth, and can even shift entire soil bacterial populations [2,4]. Another detrimental effect of crop debris is the promotion of non-pathogenic microbes that produce toxins, such as picolinic acid, salicylaldehyde or dihydroxysteric acid, making plants more susceptible to opportunistic pathogens [5]. Finally, crop debris can provide nutrients for the survival and growth of plant pathogens and other harmful soil microbes [6,7].

For ginseng, decaying roots may release ginsenosides, such as R1, Rg1, Re, Rg2, and Rd, which have been shown to inhibit ginseng seed germination and seedling growth [8]. Ginsenosides in soil can increase populations of pathogens, such as *Phytophthora cactorum*, *Pythium irregulare* and *Ilyonectria mors-panacis*, and decrease populations of beneficial microorganisms, such as *Trichoderma hamatum* and *T. harzianum*, which are antagonists of soil-borne pathogens [9–11]. Decaying ginseng roots can also release phenolic compounds such as p-hydroxybenzoic acid, vanillin, syringic acid, vanillic acid, coumaric acid, ferulic acid, cinnamic acid, salicylic acid, and benzoic acid into soil; these have been found able to inhibit the growth of ginseng [12].

When American ginseng (*Panax quinquefolius*) is planted in the same soil in which ginseng was previously harvested, crop failure can occur, which is known as replant disease [13]. Ginseng replant disease is host-specific in that other crops, such as rice, soybean, wheat and maize, can be planted in ginseng soil without being affected [14,15]. Replant disease is associated with root infections by *Ilyonectria mors-panacis*, which can cause symptoms ranging from black-brown localized lesions to disappearing root rot, where the entire root disintegrates leaving only the epidermis, which leads to wilt, discoloration, and death of the plants [13,16]. In replant disease, infections typically result in plant death, whereas plant death is much rarer in first crop soils (i.e., those not previously planted with ginseng). Ginseng replant disease has been proposed to be ultimately caused by root rot due to *I. mors-panacis* combined with an unknown host-related factor [17]. Host-related factors associated with replant disease include ginsenosides, phenolics, and aliphatic compounds that enter the soil where they can act as autotoxic allelochemicals, damaging ginseng [8,18] or act to favor root pathogens and suppress beneficial microorganisms [11,19].

Little is known about ginseng crop debris after the harvesting of ginseng. In Ontario, harvesting is typically carried out in the fall after the shoots have died, using a modified potato digger to loosen the top 30 cm of soil; this is often followed by hand-harvesting of the roots [20]. This results in crop debris of unharvested roots remaining in the soil, which will decay over time and could release root compounds into the soil. The aim of this research was to assess the amount of *P. quinquefolius* root debris following a commercial harvest, its rate of decay, and changes in soil ginsenosides as well as changes in the rhizosphere soil bacterial and fungal microbiota, including *I. mors-panacis* in roots. Soil and roots from a 3-year-old ginseng garden were collected just prior to harvest, in early fall, mid-fall, late fall, early spring, and later spring, at which time maize is routinely planted in the following year.

2. Materials and Methods

2.1. Soil and Root Collection

A three-year-old commercial ginseng garden near Windham Centre, Ontario (42.91 °N, 80.41 °W) was used, with plots of 1 m × 1 m randomly established within a 1.8 m wide bed of ginseng. Each plot was separated by 5 m. The garden was harvested by machine-digging 30 cm into the soil, followed by hand-harvesting. Prior to harvesting, the number of stems per plot was counted. Samples from five replicate plots were collected at 5 days before harvest (2 October 2018 early fall), 10 days post harvest (dph) (12 October 2018 early fall), 41 dph (12 November 2018 mid-fall), 73 dph (14 December 2018 late fall), 198 dph (18 April 2019 early spring), and 231 dph (21 May 2019 later spring, approx. planting time for maize). A different set of five plots were used per time point. At 5 days before harvest, 400 g of soil per plot was collected to a depth of 30 cm using a soil corer (2 cm diameter), then thoroughly mixed and sieved (3 × 3 mm grid) to remove roots and debris. For other time points, the five replicate plots were excavated to 30 cm, and the soil from each of the five plots was thoroughly mixed and sieved (3 × 3 mm grid) to remove roots and debris. From the sieved soil, a 400 g sample per plot was collected and stored at −20 °C. The sieved roots were washed and then stored at −20 °C.

2.2. Root Evaluation

Roots were separated into grades: spider, chunk, forked or pencil intact taproots that had a bud, and taproot pieces (>0.5 cm diameter) and fibre root pieces (<0.5 cm diameter) that lacked a bud [20]. Fresh weight was determined after rinsing the roots and removing excess moisture with paper towels. Dry weight was determined after drying the roots at 60 °C for 72 h. Dark brown sunken lesions on each root were counted. Association of lesions with *I. mors-panacis* infection was determined by excising 0.3 × 0.3 × 0.3 mm cubes from lesions, extracting DNA, and testing for the presence of *I. mors-panacis* by submitting them to Laboratory Services, University of Guelph, for *I. mors-panacis* detection PCR using the primers CDU1/CDL1b [21].

2.3. Soil DNA Extraction and Sequencing

Soil DNA was extracted using a DNeasy PowerLyzer PowerSoil Kit (QIAGEN, Toronto, ON, Canada) according to manufacturer's instructions with modifications. Briefly, 300 mg of sieved frozen soil was added to a PowerBead tube, and mixed with solution C1 pre-heated to 60 °C. Solutions C2 and C3 were added, and the tube was incubated for 15 min at 60 °C. Samples were eluted twice with 33 µL of C6 solution added to the MB spin column. DNA concentration and purity were assessed spectrophotometrically (NanoDrop 1000, Thermo Scientific, Wilmington, DE, USA). Samples with a 260:280 nm absorbance ratio between 1.8 and 2.0 were used for sequencing.

Sequencing was performed at the Génome Québec Innovation Centre at McGill University (Montreal, QC, Canada) using an Illumina MiSeq PE250. For bacteria, 250 bp paired-end sequencing with primers 341F (CCTACGGGNGGCWGCAG) and 805R (GAC-TACHVGGGTATCTAATCC) was performed to obtain the V3-V4 region of the 16S rRNA. For fungi, 250 bp paired-end sequencing with primers ITS1F (CTTGGTCATTTAGAG-GAAGTAA) and ITS2R (GCTGCGTTCTTCATCGATGC) was used for the ITS1 region.

2.4. Microbial Diversity and Abundance

Paired-end reads were joined and filtered for quality, the Fluidigm adaptors (ACACT-GACGACATGGTTCTACA and TACGGTAGCAGAGACTTGGTCT) were trimmed, and singletons and duplicated sequences removed using 32-bit USEARCH software (USEARCH v11.0.667, http://drive5.com/uparse/) accessed 1 February 2019 [22]. The reads were then demultiplexed to remove the index adapters from the reads (demux command), and de-noised to remove unlikely/low count reads to improve overall quality of the mapping using the DADA2 plugin [23], with the truncation argument set up to 280 nt and 220 nt for the forward and reverse ends, respectively; the reads were trimmed to 10 nt from both ends.

For bacteria, the OTUs were annotated using the 16S/18S rRNA database of SILVA non-redundant NR99 SSU v132 (https://www.arb-silva.de/) accessed 15 February 2019 [24], with a 97% identity cutoff using the SINTAX command in USEARCH. For fungi, the OTUs were annotated using the fungal ITS taxonomy file from the UNITE v8.0 database [25]. OTUs were assigned to the deepest taxonomic level available. Taxonomic designations were confirmed by aligning OTUs in each phylum with sequences of related taxa from GenBank using MUSCLE v3.8.31 [26], and a maximum likelihood phylogram was generated using RAxML v8.2.12 [27] using the GTRGAMMA substitution model, and viewed in MEGA 7.0.26 (https://megasoftware.net/) accessed 1 March 2019 [28] to check each OTU for their taxonomic assignment.

OTU abundance was determined by mapping the reads to the OTUs using the alignment program bowtie2 v2.3.4.1 (http://bowtie-bio.sourceforge.net/bowtie2/index.shtml) accessed 1 March 2019 [29] to obtain the number of reads per OTU. OTU abundance was determined using RSEM v1.3.1 (http://deweylab.github.io/RSEM/) accessed 5 March 2019 [30] with SAMtools v1.7 (http://samtools.sourceforge.net/) accessed 5 March 2019 [31] using the script util/align_and_estimate_abundance.pl, which is part of the Trinity v2.8.5 package (https://github.com/trinityrnaseq/trinityrnaseq) accessed 5 March 2019 [32]. Trimmed Means of M-values (TMM) were determined for cross-sample comparison using the R package edgeR v3.20.9 [33,34] in R v3.4.4 x86_64-pc-linux-gnu (https://www.r-project.org/) accessed 10 March 2019 by averaging OTU abundance after removing 30% of both the lower and upper ranges of the log-abundance (M-value) and 5% of the absolute abundance values (A-value) [33]. Percent OTU abundance per dph was calculated by dividing the number of OTUs per taxon by the total number of OTUs.

2.5. Cluster Analysis

Clusters were created using the K-means clustering algorithm in the R Stats Package v. 3.6.2 (http://www.r-project.org/) accessed 16 April 2019 [35]. The centroid for each cluster was created from the average of the OTU percent abundance.

2.6. Soil Ginsenosides

Soil ginsenoside extraction was carried out via a modified methanol (MeOH) method [8]. Air-dried soil (20 g) was shaken in 60 mL 80% MeOH at 175 rpm for 24 h, and then filtered (P4 filter paper; Fisher Scientific, Mississauga, ON, CA). The filtrate was dried under a vacuum at 40 °C, and then suspended in 1 mL 80% MeOH and stored at −20 °C. Ginsenosides were separated per Ivanov et al. [36], with minor modifications. A ZORBOX Eclipse Plus C8 column (2.1 × 50 mm, 1.0 μm, Agilent Technologies, Santa Clara, CA, USA) was used with initial conditions of 25% solvent B (90% acetonitrile, 0.1% formic acid, 1 mg/L sodium acetate): 75% solvent A (0.1% formic acid, 1 mg/L sodium acetate) for 1 min, followed by a linear gradient to 35% solvent B over 2 min, then 95% solvent B over 6 min, and finally, 95% solvent B for 1 min, before returning to the initial conditions. The flow rate was 0.4 mL/min, and the eluent monitored at 203 nm before infusion into an Agilent 6320 TOF mass spectrometer through a dual-spray electrospray ionization (ESI) source with a gas temperature of 325 °C flowing at 12 L/min, and a nebulizer pressure of 45 psi. The fragmentor voltage was set to 120 V with a Vcap of 4500 V. Automated internal calibration was carried out using reference ions 121.0508 and 922.0096. Ginsenosides were detected as their Na^+ adducts, in positive ion mode (M+Na+H).

2.7. Soil Characterization

For soil texture, three 100 g soil samples were randomly sampled from the plots and then air-dried and combined. Particle size was determined using method SNL-027 [37].

2.8. Data Analysis

Analysis was performed with PROC GLM in SAS 9.1 (SAS Institute Inc., Cary, NC, USA). If the analysis of variance showed statistically significant differences per root grade between sampling times ($p < 0.05$), then means were compared with Fisher's protected least-significant-difference test ($p = 0.05$).

3. Results

3.1. Soil Characterization

The soil of the plots was determined to be sand (77.9%), very fine sand (14.5%), fine sand (34.4%), medium sand (23.6%), coarse sand (4.2%), very coarse sand (1.2%), silt (15.5%), and clay (6.5%).

3.2. Root Number and Biomass

Prior to harvest, there were 62 ± 2.1 (mean $\pm$ SD) stems per m^2, whereas there were 22.0 ± 5.5 taproots with buds per m^2 at 10 days after harvest, indicating that approximately 35% of the taproots were not harvested, based on five replicate 1 m × 1 m plots fully sampled to a 30 cm depth. Total root number declined progressively after harvest, with 83.7, 52.7, 16.3 and 1.5% of the 10 dph total root number (excluding fibre root pieces) remaining at 41, 73, 198 and 231 dph, respectively (Figure 1A). The steepest decline per day was between 41 and 73 dph. Based on number, small fibre root pieces dominated the root grades at 10 dph at 147.8 per m^2, but none were detectable by the next sampling date at 41 dph. The next most common root grade at 10 dph was pencil-shaped taproots, with the greatest decline per day between 10 and 43 dph, followed by chunk-shaped taproots, which declined most rapidly per day between 10 and 73 dph. Taproot piece number increased between 10 and 43 dph due to many intact taproots being partially decayed with the loss of the bud, and hence being graded as taproot pieces. Spider- and fork-shaped taproots were relatively rare at 10 dph, with spider-shaped taproots no longer detectable by 73 dph and fork-shaped taproots no longer detectable by 231 dph. By 231 dph, only a few taproot pieces with disappearing root rot symptoms and a few healthy-looking germinating intact pencil-shaped taproots remained.
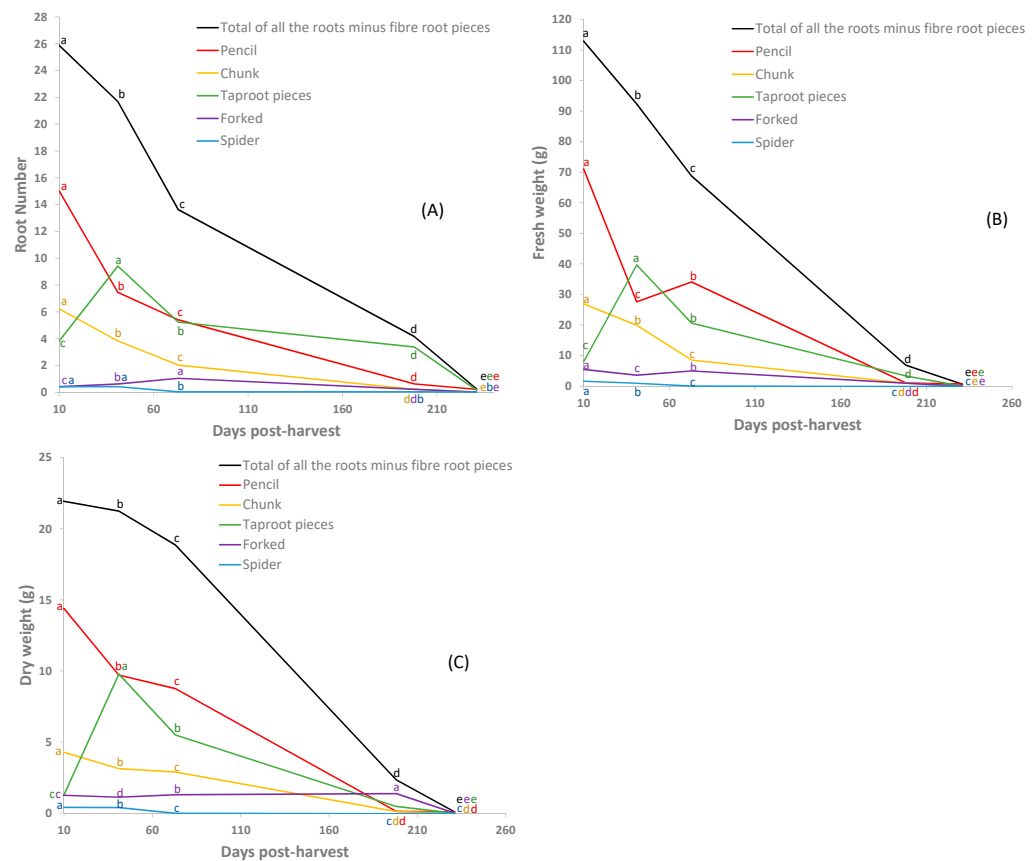
Figure 1. Biomass of ginseng roots after harvest. (**A**) Number of ginseng roots; (**B**) Fresh weight (g) of ginseng roots; (**C**) Dry weight (g) of ginseng roots. Each point represents the average number for total roots (not including fibre root pieces) and different root grades per five 1 m^2 × 0.3 m deep plots from 10 to 231 days post-harvest (dph). An ANOVA followed by Fisher's protected least-significant-difference test ($p < 0.05$) was used to calculate significant differences between means between time points within each root grade, and letters not in common show significantly different means.

At 10 dph, total root fresh weight was 115.4 g per m^2. Based on an estimated average fresh weight yield of 1.2 kg roots per m^2 of a typical ginseng garden in southern Ontario (Sean Westerveld, personal communication), approximately 7.8% of total root fresh weight was not harvested in this garden. This was much less than the estimated 35% root number not harvested mentioned previously, indicating that many of the non-harvested roots were relatively small. Total root fresh weight declined almost linearly after harvest, except for a slower decline between 198 and 231 dph, with 79.9, 59.4, 5.8 and 0.7% of the 10 dph total fresh root weight at 41, 73, 198 and 231 dph, respectively (Figure 1B). Among the root grades, pencil-shaped taproots had the greatest fresh weight at 10 dph, with the greatest per day decline between 10 and 41 dph, followed by chunk-shaped taproots, which declined most rapidly between 10 and 73 dph. As buds were lost on intact taproots as they became partially degraded, they were reclassified as taproot pieces. This could explain why the taproot-grade fresh weight increased from 10 to 43 dph. Spider- and fork-shaped taproot grades had the lowest fresh weights among various root types at 10 dph, and then declined over time. Fibre root pieces were only 2.6 g per m^2 at 10 dph.

At 10 dph, total root dry weight was 22.7 g per m^2, and the roots were 19.7% dry matter. Total root dry weight declined progressively over time, most rapidly on a per day basis between 73 and 198 dph, with 93.6, 82.5, 10.2 and 0.5% of the 10 dph total dry root weight at 41, 73, 198 and 231 dph, respectively (Figure 1C). Pencil-shaped taproots followed by chunk-shaped taproots had the highest dry weights at 10 dph, declining most rapidly per day between 10 and 41. The dry weights of the other root grades were lower at 10 dph, and all declined over time, except for an increase in dry weight for taproot pieces between

10 and 41 dph, related to their increased number. The dry weight of fibre root pieces was only 0.8 g per m^2 at 10 dph.

3.3. Root Lesions

At 10 dph, 5.8% of all the roots had lesions (1.5 roots with lesions per m^2), with no lesions observed on pencil-shaped taproots or fibre root pieces. Total root numbers with lesions were 4.1 fold, 2.1 fold and 2.3 fold higher than the 10 dph total at 41, 73 and 198 dph, respectively (Figure 2A). At 231 dph, no roots with defined lesions were detectable, as none of the remaining pencil-shaped roots showed lesionsm and all the remaining taproot pieces (0.2 roots per m^2) had symptoms of disappearing root rot instead of defined lesions. Chunk, pencil and taproot pieces had the highest lesion numbers at 10 dph, declining over time, but taproot pieces always had the most lesions compared to intact taproots. Spider and forked-shaped taproots had only a few lesions at 10 dph, and none were detected later, except on forked-shaped taproots at 198 dph.
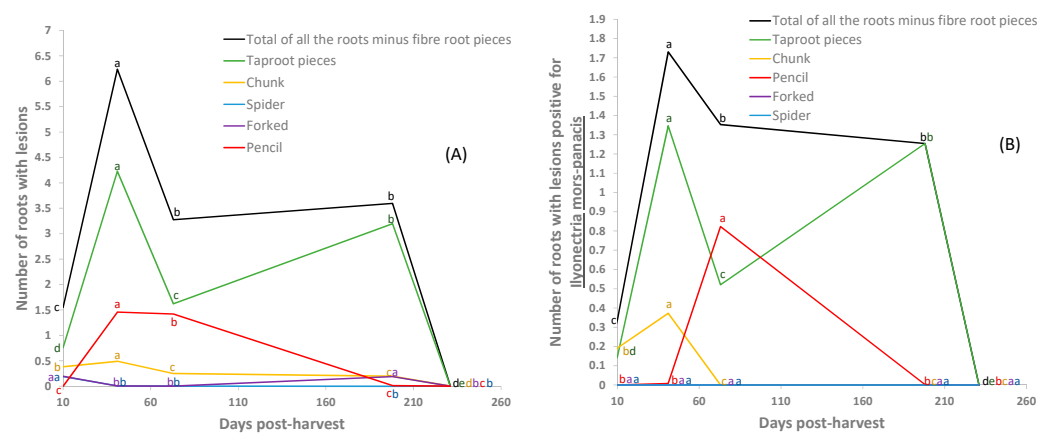

Figure 2. Lesions on ginseng roots after harvest. (**A**) Number of roots with lesions. (**B**) Number of roots with lesions positive for *Ilyonectria mors-panacis*. Each point represents the average number for total roots (not including fibre root pieces) and different root grades per five 1 m^2 × 0.3 m deep plots from 10 to 231 days post-harvest (dph). An ANOVA followed by Fisher's protected least-significant-difference test ($p < 0.05$) was used to calculate significant differences between means between time points within each root grade, and letters not in common show significantly different means.

Among all the root lesions at 10 dph, 22% were associated with *I. mors-panacis*. The total number of roots with lesions associated with *I. mors-panacis* was 5.1 fold, 4.0 fold and 3.7 fold higher than the 10 dph value at 41, 73 and 198 dph, respectively (Figure 2B). At 231 dph, no lesions associated with *I. mors-panacis* were detectable, since DNA could not be extracted from the disintegrating taproot pieces affected by disappearing root rot, and thus the pathogen could not be detected via PCR. Except at 10 dph for chunk-shaped roots and 41 dph for pencil-shaped roots, lesions associated with *I. mors-panacis* were only found in taproot piece roots.

3.4. Soil Ginsenosides

Four PPD-type ginsenosides (Rb1, Rd, GXVII, Rc+Rb2) were detected in the soil (Figure 3A). Rc+Rb2 were grouped together, as their peaks in HPLC could not be distinguished from each other. At −5 dph, 61% of the total PPD-type ginsenosides were Rb1, 24% were Rd, 9% were GXVII, and 6% were Rc+Rb2. Total PPD ginsenosides declined from −5 to 198 dph, with an increase between 198 and 231 dph. The fastest decline was between −5 and 10 dph, dropping 3.42×10^4 AU per day compared to the second fastest at 2.94×10^3 AU per day between 73 and 198 dph. Changes in amounts of the individual PPD ginsenosides generally followed the pattern for total PPD-type ginsenosides, except for GXVII, where there were no significant changes between −5 and 73 dph.
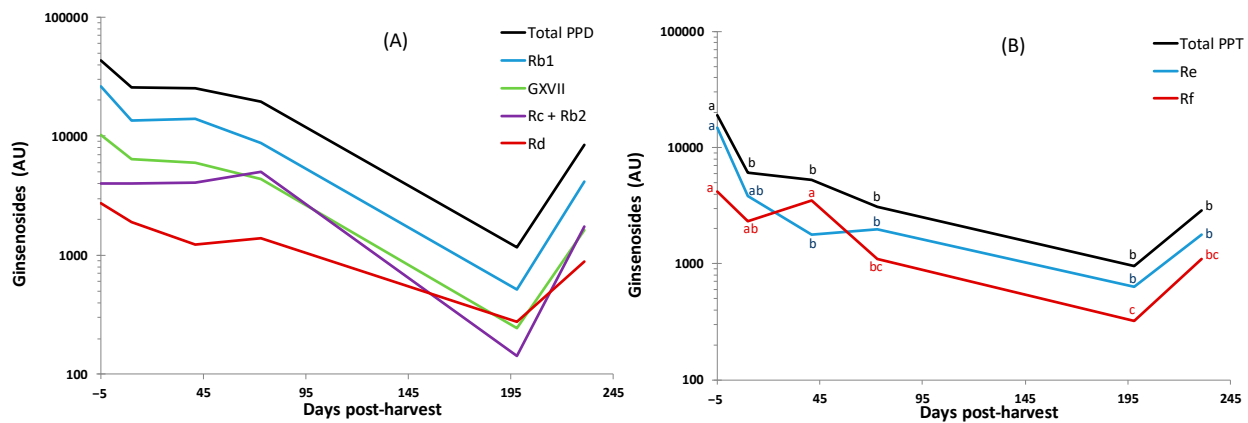
Figure 3. Changes in total and individual ginsenosides detected in soil. (**A**) Total PPD ginsenosides and individual PPD ginsenosides (Rb1, Rd, GXVII and Rc+Rb2). (**B**) Total PPT ginsenosides and individual PPT ginsenosides (Re and Rf). Each point represents the average amount of ginsenosides per g soil in five 1 m^2 × 0.3 m deep plots from 10 to 231 days post-harvest (dph). Bars represent standard deviation. An ANOVA followed by Fisher's protected least-significant-difference test ($p < 0.05$) was used to calculate significant differences between means of different time points within each group, and letters not in common should significantly different means.

Two PPT-type ginsenosides (Re and Rf) were detected in the soil, with 78% composed of Re and 22% composed of Rf at −5 dph (Figure 3B). Total PPT ginsenoside declined from −5 to 198 dph, and then increased between 198 and 231 dph. Total PPT ginsenosides declined most rapidly between −5 and 10 dph at 2.57×10^4 AU per day compared to the second fastest decline between 73 and 198 dph at 3.37×10^2 AU per day. The pattern of changes in the individual PPT ginsenosides was similar to that of total PPT-type ginsenosides, with the notable exception of an increase at 41 dph in Rf.

3.5. Soil Bacterial OTUs

For the six time points from fall to spring with five replicate plots, each sequenced separately, almost five million reads were generated from the 30 samples. Over 7000 bacterial OTUs based on matches to the 16S RNA were detected, and these were found to belong to 21 phyla. Based on the number of reads per phylum, members of the Proteobacteria and Actinobacteria were most abundant, making up 53.5 and 38.7% of the reads, respectively, followed by Chloroflexi, Firmicutes and Acidobacteria, with 9.9, 6.0 and 5.8% of the reads, respectively, and Planctomycetes, Gemmatimonadetes, and Bacteroidetes, with 2.4%, 1.9% and 0.9% reads, respectively. The other 13 phyla were rare, together making up less than 1.0% of the reads (Figure 4).

The genus-level bacterial OTUs were separated into nine clusters based on the patterns of changes in OTU abundance over time (Figure 4 and Figure S1 and Tables S1–S10). The notable characteristic of the centroid of cluster 1 with 4 OTUs was a peak in abundance at −5 dph; of the centroid of cluster 2 with 8 OTUs was a peak at 10 dph; of the centroid of cluster 3 with 5 OTUs was a peak at 41 dph; of the centroid of cluster 4 with 11 OTUs was a peak at 41 dph (like cluster 3, but with a smaller peak height); of the centroid of cluster 5 with 8 OTUs was a peak at 73 dph, of the centroid of cluster 6 with 13 OTUs was a drop at 41, 73, and 231 dph; of the centroid of cluster 7 with 5 OTUs was a drop between 10 and 73 dph; and of the centroid of cluster 8 with 12 OTUs was a peak at 231 dph (Figure 4). These peaks and drops of the centroid were all significant, relative to other time points in their respective cluster (Tables S1–S8). Clusters 1 to 8 were dominated by Proteobacteria (28 OTUs) and Actinobacteria (25 OTUs), with much fewer Firmicutes (7 OTUs) and Acidobacteria (3 OTUs). Members of cluster 9 contained OTUs with relatively low abundances compared to the other clusters, and this was the only cluster containing OTUs that belonged to both previously described genera (142 OTUs) and non-described genera (161 OTUs) (Tables S9 and S10). The centroid of cluster 9 was relatively flat over time, with only a significant difference at −5 dph

in the centroid of cluster 9 for previously described genera (Figure S1, Tables S9 and S10). Almost all of the OTUs in cluster 9 were undetectable at one or more time points, and cluster 9 had OTUs belonging to all 21 bacterial phyla.
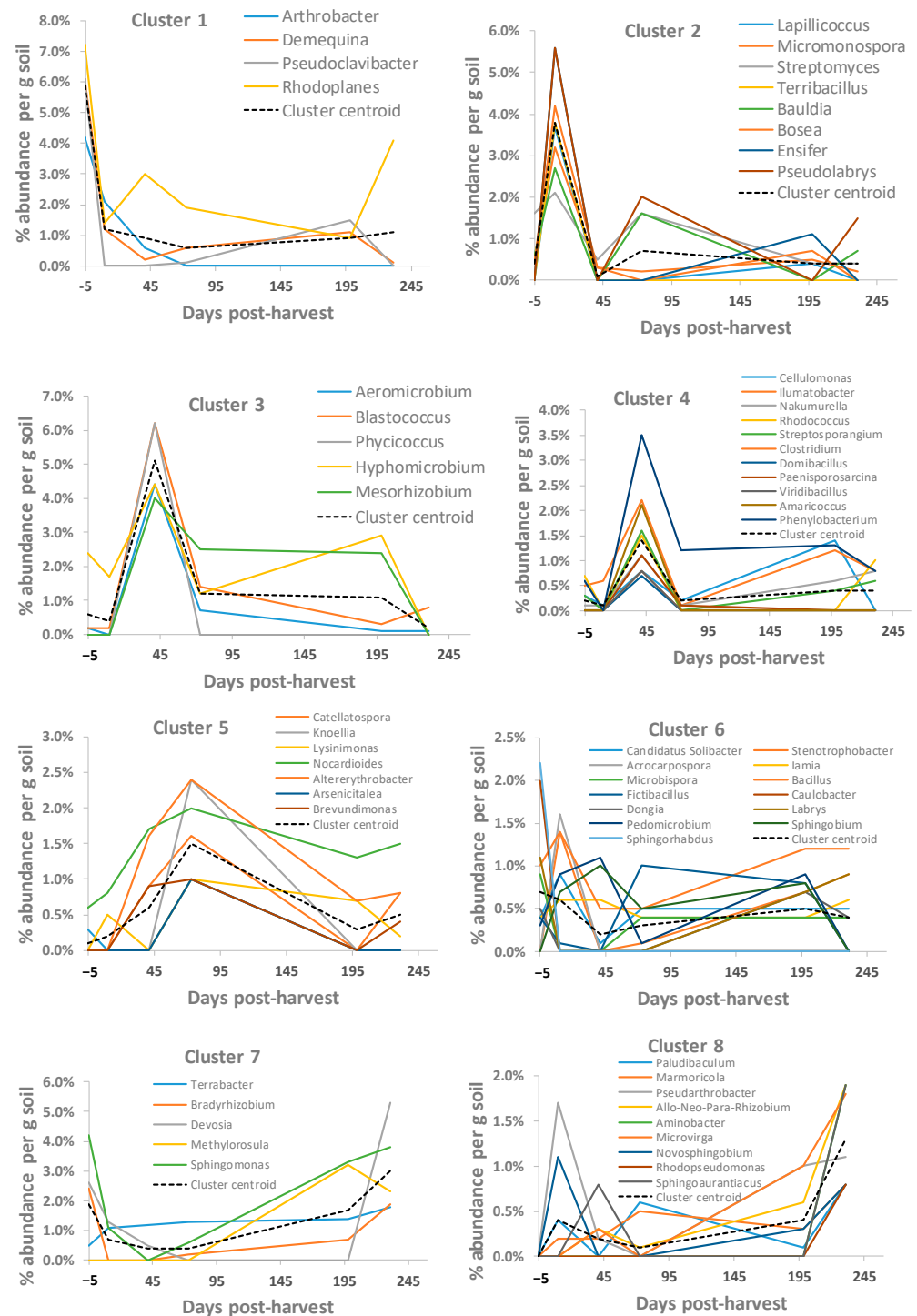

Figure 4. Bacterial genus-level clusters 1 to 8 of OTU abundance over time. Percentage abundance per total OTUs at each time point. Each point represents the average percentage abundance per total OTUs per g soil in five 1 m² × 0.3 m deep plots from 10 to 231 days post-harvest (dph). Genus names for OTUs identified based on 97% nt identity of the 440–476 bp V3–V4 region of the 16S rRNA using USEARCH with the SILVA 132 SSU NR99 database (https://www.arb-silva.de/) accessed 25 April 2019. Clusters were created with a K-means clustering algorithm in R, separating OTU abundance over dph [35]. The cluster centroid was created using the average within each K-means cluster.

3.6. Soil Fungal OTUs

For the six time points from fall to spring with five plots, almost four million fungal reads were generated from the 30 samples. Fungal OTUs were detected belonging to seven phyla. The most abundant was Ascomycota with 35.1% of the reads, followed by Mortierellomycota, Basidiomycota, Rozellomycota, Zoopagomycota, and Chytridiomycota with 24.2%, 19.7%, 9.3%, 8.8% and 2.7% of the reads, respectively. The Mucoromycota was rare with only 0.1% of the reads.

The genus-level fungal OTUs were separated into ten clusters based on the pattern of changes in OTU abundance over time (Figure 5 and Figure S2, Tables S11–S20). Clusters 1 to 3 only contained a single OTU each. The centroid of cluster 1 showed a peak at 198 dph, significantly greater than values at −5 and 10 dph, and was composed of the Ascomycete *Plenodomus* (Figure 5 and Table S11). The centroid of cluster 2 was highest at 10 dph, followed by decline and then an increase at 231 dph, both of which were not significantly greater than the other values, and was composed of the Ascomycete *Trichoderma* (Figure 5 and Table S12). The centroid of cluster 3 showed peaks at 73 and 231 dph that were significant, and was composed of the Basidiomycete *Subulicystidium* (Figure 5 and Table S13). The notable characteristic of the centroid of cluster 4 with 6 OTUs was a peak at 10 and 41 dph and an increase at 231 dph, but these were not significant; the centroid of cluster 5 with 11 OTUs showed small peaks at 10 and 231 dph that were not significant, with OTU abundances generally below 1%. The centroid of cluster 6 with 7 OTUs had a peak at 10 dph that was significantly greater than values at 41, 198, and 231 dph; the centroid of cluster 7 with 5 OTUs had a peak at −5 dph, but that was not significant, and the centroid of cluster 8 with 3 OTUs had a peak at 73 dph that was significantly higher than other time points (Figure 5 and Tables S14–S18). Clusters 9 and 10 contained OTUs with relatively low abundances, generally below 1%. The centroids of cluster 9 with 32 OTUs and cluster 10 with 87 OTUs were relatively flat, with no significant differences over time (Figure S2, Tables S19 and S20). All the OTUs in clusters 9 and 10 were undetectable at one or more time points. Clusters 4 to 10 were dominated by Ascomycota (95 OTUs) and Basidiomycota (33 OTUs), with much fewer Chytridiomycota (9 OTUs) and only 1 OTU each of the Mortierellomycota, Rozellomycota, Mucoromycota and Zoopagomycota.
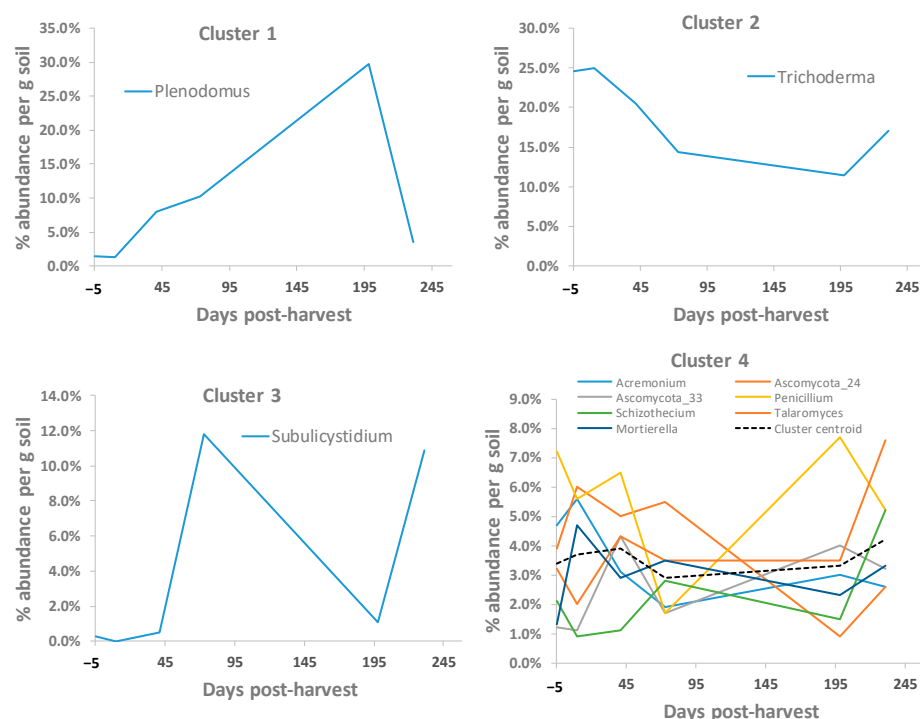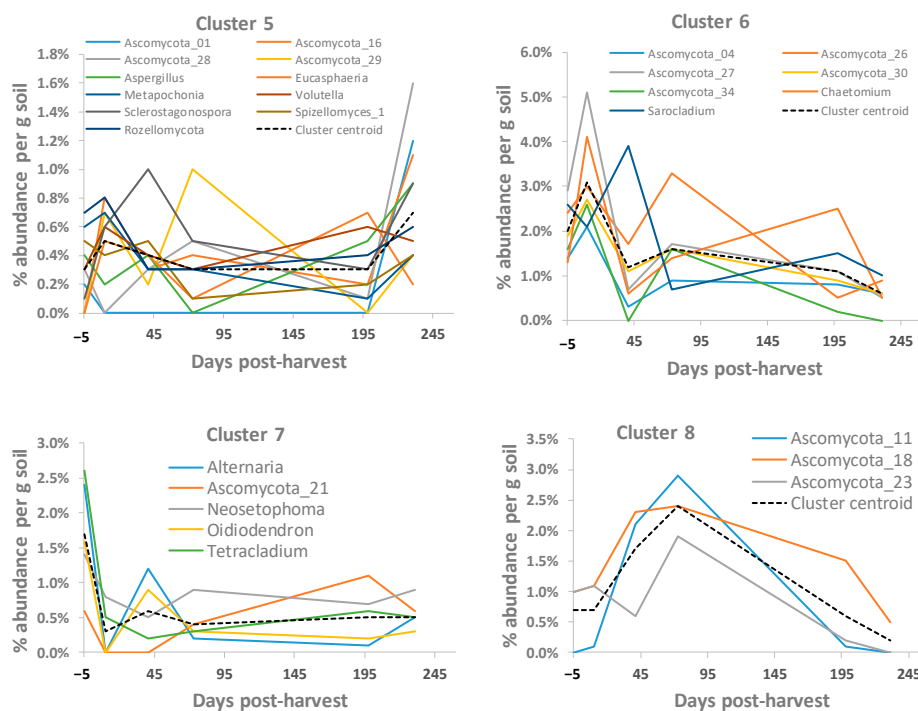

Figure 5. *Cont.*

Figure 5. Fungal genus-level clusters 1 to 8 of OTU abundance over time. Percentage abundance per total OTUs at each time point. Each point represents the average percentage abundance per total OTUs per g soil in five 1 m^2 × 0.3 m deep plots from 10 to 231 days post-harvest (dph). Genus names for OTUs identified based on 97% nt identity of the 220–280 bp ITS2 region of the 18S rRNA using QIIME 2 with the UNITE v8.0 database (release 2019.10, https://QIIME2.org/) https://www.arb-silva.de/) accessed 30 April 2019. Clusters were created using a K-means clustering algorithm in R, separating OTU abundance over dph [35]. The cluster centroid was created using the average within each K-means cluster.

4. Discussion

For commercial ginseng gardens in Ontario, harvesting is preceded by removing the straw mulch and dead stems and leaves, and then digging 30 cm into the soil with a modified potato harvester to expose roots that are most often collected manually [20]. Harvesting concentrates on the most valuable roots, whereas many lower-market-value roots, such as damaged and rotted taproot pieces and fibre roots, are less likely to be collected. Smaller roots are also likely to pass through the harvester and thus not be harvested as they are reburied in the soil. In this study, there was considerable amount of post-harvest root debris, with mostly smaller pencil taproots, taproot pieces, and fibre root pieces remaining after harvest. As the taproot and fibre root pieces appeared to have relatively fresh wounds at 10 dph, most of the wounds were likely generated during harvesting.

Based on the speed of decay, fibre root pieces were the most readily decayed, becoming no longer detectable by 41 dph. Fibre root pieces may be more susceptible to decay due to their small diameter and high starch and fatty acid contents [38]. In contrast, several intact pencil-shaped roots were found without any signs of decay at 231 dph, with buds starting to germinate, and thus would have continued to grow as volunteer plants. The lack of lesions on them may indicate that they are more resistant to microbial decay, but they may simply be escapes from decay. Such roots should be further investigated to assess if they have greater resistance to root rot diseases, including replant disease. Isutsa and Merwin [39] reported resistance to apple replant disease in seven rootstocks of interspecific hybrids, with resistance or tolerance to root rot caused by species of *Rhizoctonia*, *Pythium* and *Fusarium*.

An average of 36% of the lesions observed on roots were associated with *I. mors-panacis*, indicating that root debris after harvest became a nutrient source for the fungus, increasing

the inoculum of the pathogen in the soil. This is significant as *I. mors-panacis* is associated with root rot in replant disease [40]. Differences in infection rates between root grades could possibly reflect genetic differences between roots related to susceptibility to *I. mors-panacis*. No spider or forked-shaped roots were observed with lesions associated with *I. mors-panacis*, and no pencil-shaped roots had such lesions until 73 dph. In contrast, taproot pieces, which would have wounds as they are missing buds, appeared to be most susceptible, with lesions associated with *I. mors-panacis* at all time points except 231 dph. However, the majority of lesions on all roots were not associated with *I. mors-panacis*, indicating that populations of other ginseng root rot organisms were also increasing in the debris. Lesion incidence was highly related to wounding, with the percentage of lesions on wound sites of taproot pieces at 100% (10 dph), 73% (41 dph), 77% (73 dph) or 87% (198 dph), indicating the importance of an intact epidermis in root rot resistance.

In addition to lesion numbers, lesion appearance also changed over time. During the fall and early spring, the severity of root rot associated with *I. mors-panacis* was less, with mostly smaller dark brown lesions with defined edges. However, at 231 dph, taproot pieces had no distinguishable lesions, because they were completely decayed with symptoms of disappearing root rot. Thus, severe root rot symptoms first appeared in late spring following harvest.

Both the total PPD-type and the PPT-type ginsenoside contents in soil declined during the fall, although Rb1, Rd and Rf levels fluctuated during the fall, and then all ginsenoside types declined over winter. One explanation for the decrease in ginsenoside content in the soil is the deglycosylation of major ginsenosides (Rb1, Rb2, Rd, Rc and Re), which has been reported to be caused by many ginseng soil microbes [41]. Surprisingly, ginsenoside content in the soil increased during spring. One possibility is that they were produced by soil microbes, such as the *Fusarium*, *Aspergillus* and *Verticillium* isolated from *P. ginseng* roots, which can produce ginsenosides in potato dextrose broth [42]. However, the increase could also be due to their release from soil particles, dead soil microbes, or from the remaining decayed roots during warmer spring temperatures.

For soil bacteria in this study, nine clusters could be created from the patterns of changes in abundance over time, and seven of those clusters showed statistically significant differences at least at one time point. A peak in abundance at -5 dph (clusters 1 and 6) possibly indicates the preference of those bacteria for growth in the intact rhizosphere prior to harvest; a peak at 10 dph (clusters 2 and 6) possibly indicates a preference for disrupted soil due to harvesting; a peak at 41 dph (clusters 3 and 4) possibly indicates a preference for nutrients released relatively early in root and straw decay with milder fall temperatures; a peak at 73 dph (cluster 5) possibly indicates a preference for nutrients released later in root and straw decay with cooler fall temperatures; a peak at 198 dph (clusters 6 and 7) may indicate a preference for freezing and thawing soil during winter or perhaps the release of nutrients during warming in early spring; and a peak at 231 dph (clusters 7 and 8) may indicate a preference for milder and higher late-spring temperatures. While the reasons for different peaks in abundance requires further investigation, the results showed that bacterial populations can change in the soil related to changes in their environment following harvest.

For soil fungi in this study, ten clusters could be made from the patterns of changes in abundance over time, and five clusters showed statistically significant differences at least at one time point. Three of those clusters contained only a single highly abundant out, either *Plenodomus*, *Trichoderma* or *Subulicystidium*, which were the three fungal genera that dominated fungal abundance in this study. The other clusters with significant differences in abundance over time were cluster 6, with a peak at 10 dph relative to 41, 198, and 231 dph, and cluster 8, with a peak at 73 dph relative to all other time points. Like the bacterial soil populations, the changes in fungal abundance could be related to the nutrient or environmental conditions at a particular time point. However, most fungal clusters showed no clear peaks in fungal OTU abundance after harvesting.

One element that could be affecting the microbial population would be the release of ginsenosides as the roots decay. Ginsenosides comprise 3–8% dry weight of ginseng roots [43], and so the 22.7 g dry weight of total root per 1 m^2 observed in the early fall (10 dph) in this study could possibly have resulted in the release of a relatively large amount (0.6–1.8 g) of ginsenosides into a 1 m^2 soil area. Adding a ginsenoside mixture into soil decreased populations of beneficial fungi, such as species of *Acremonium*, *Mucor* and *Ochroconis*, but increased populations of known pathogenic fungi, such as species of *Alternaria*, *Cylindrocarpon*, *Gibberella*, *Phoma* and *Fusarium* [11]. Park et al. [44] noted that there was a large variety of *P. ginseng* soil bacteria and fungi with glycosidases that could remove sugars from ginsenosides. Ginsenosides were considered to be the main substances driving changes in the soil microbiome of *P. notoginseng,* acting as a carbon source for some members of the soil microbiome, stimulating growth while acting as inhibitors of other microbes [45]. While soil ginsenoside contents declined after harvest, this could be related to their uptake by certain soil microbes [9], and the death of those microorganisms due to freezing and thawing over winter could have released them into the soil, resulting in the increased soil ginsenosides observed in spring.

5. Conclusions

While there have been many studies of the soil microbiome of ginseng, such as the impact of fungicides, mulches and shading [46], this is the first to examine the impact of harvesting. This study found that there was a relatively large amount of root biomass after harvesting debris, with decay occurring throughout the fall as indicated by decreasing numbers of roots, increasing numbers of taproot pieces, and increasing numbers of lesions per root. By late spring, only a few roots that were taproot pieces remained; these had symptoms of disappearing root rot or were healthy-looking germinating pencil-shaped taproots. There were many bacterial OTUs, with groups showing elevated populations at particular periods after harvest, but this was less obvious with fungi, which were heavily dominated by three taxa. Thus, the process of commercial ginseng harvesting and the decay of ginseng root debris impacts both pathogenic and non-pathogenic soil microorganisms as well as soil ginsenosides, all of which have been proposed to be important in the establishment of ginseng replant disease.

Supplementary Materials: The following supporting information can be downloaded at: https://www.mdpi.com/article/10.3390/soilsystems7040108/s1, Figure S1: Bacterial genus-level cluster 9 of OTU abundance at just prior −5 dph and after harvest 10, 41, 73, 198 and 231 dph. Figure S2: Fungal genus-level clusters 9 and 10 of OTU abundance over time at just prior −5 dph and after harvest 10, 41, 73, 198 and 231 dph; Table S1: Comparison of bacterial genus-level cluster 1 of OTU abundance over time; Table S2: Comparison of bacterial genus-level cluster 2 of OTU abundance over time; Table S3: Comparison of bacterial genus-level cluster 3 of OTU abundance over time; Table S4: Comparison of bacterial genus-level cluster 4 of OTU abundance over time; Table S5: Comparison of bacterial genus-level cluster 5 of OTU abundance over time; Table S6: Comparison of bacterial cluster 6 of OTU abundance over time; Table S7: Comparison of bacterial genus-level cluster 7 of OTU abundance over time; Table S8: Comparison of bacterial genus-level cluster 8 of OTU abundance over time; Table S9: Comparison of bacterial cluster 9 OTU for described bacteria at genus level over time; Table S10: Comparison of bacterial cluster 9 OTU for unidentified bacteria at genus level over time; Table S11. Comparison of fungal cluster 1 OTU abundance over time; Table S12. Comparison of fungal cluster 2 OTU abundance over time; Table S13. Comparison of fungal cluster 3 OTU abundance over time; Table S14. Comparison of fungal cluster 4 OTU abundance over time; Table S15. Comparison of fungal cluster 5 OTU abundance over time; Table S16. Comparison of fungal cluster 6 OTU abundance over time; Table S17. Comparison of fungal cluster 7 OTU abundance over time; Table S18. Comparison of fungal cluster 9 OTU abundance over time; Table S19: Comparison of fungal cluster 9 OTU abundance over time; Table S20: Comparison of fungal cluster 10 OTU abundance over time.

References

1. Batish, D.R.; Singh, H.P.; Kaur, S. Crop allelopathy and its role in ecological agriculture. *J. Crop Prod.* **2001**, *4*, 121–161. [CrossRef]
2. Cipollini, D.; Rigsby, C.M.; Barto, E.K. Microbes as targets and mediators of allelopathy in plants. *J. Chem. Ecol.* **2012**, *38*, 714–727. [CrossRef] [PubMed]
3. Yang, J.I.; Ruegger, P.M.; McKenry, M.V.; Becker, J.O.; Borneman, J. Correlations between root-associated microorganisms and peach replant disease symptoms in a California soil. *PLoS ONE* **2012**, *7*, e46420. [CrossRef]
4. Zhou, X.; Wu, F. P-coumaric acid influenced cucumber rhizosphere soil microbial communities and the growth of *Fusarium oxysporum f.* sp. *cucumerinum* Owen. *PLoS ONE* **2012**, *7*, e48288.
5. Patrick, Z.A.; Toussoun, T.A.; Koch, L.W. Effect of crop-residue decomposition products on plant roots. *Annu. Rev. Phytopathol.* **1964**, *2*, 267–292. [CrossRef]
6. Almeida, Á.M.R.; Saraiva, O.F.; Farias, J.R.B.; Gaudêncio, C.A.; Torres, E. Survival of pathogens on soybean debris under no-tillage and conventional tillage systems. *Pesqui. Agropecu. Bras.* **2001**, *36*, 1231–1238. [CrossRef]
7. Krupinsky, J.M.; Bailey, K.L.; McMullen, M.P.; Gossen, B.D.; Turkington, T.K. Managing plant disease risk in diversified cropping systems. *Agron. J.* **2002**, *94*, 198–209. [CrossRef]
8. Yang, M.; Zhang, X.; Xu, Y.; Mei, X.; Jiang, B.; Liao, J.; He, X. Autotoxic ginsenosides in the rhizosphere contribute to the replant failure of *Panax notoginseng*. *PLoS ONE* **2015**, *10*, e0118555. [CrossRef]
9. Nicol, R.W.; Yousef, L.; Traquair, J.A.; Bernards, M.A. Ginsenosides stimulate the growth of soilborne pathogens of American ginseng. *Phytochemistry* **2003**, *64*, 257–264. [CrossRef]
10. Bernards, M.A.; Yousef, L.F.; Nicol, R.W. The allelopathic potential of ginsenosides. In *Allelochemicals: Biological Control of Plant Pathogens and Diseases*; Mukerji, K.G., Ed.; Springer: Dordrecht, The Netherlands, 2006; pp. 157–175.
11. Li, Y.; Dai, S.; Wang, B.; Jiang, Y.; Ma, Y.; Pan, L.; Wu, K.; Huang, X.; Zhang, J.; Cai, Z.; et al. Autotoxic ginsenoside disrupts soil fungal microbiomes by stimulating potentially pathogenic microbes. *AEM* **2020**, *86*, e00130-20. [CrossRef]
12. Bi, X.B.; Yang, J.X.; Gao, W.W. Autotoxicity of phenolic compounds from the soil of American ginseng (*Panax quinquefolium* L.). *Allelopath. J.* **2010**, *25*, 115–122.
13. Reeleder, R.D.; Roy, R.; Capell, B. Seed and root rots of ginseng (*Panax quinquefolius* L.) caused by *Cylindrocarpon destructans* and *Fusarium* spp. *J. Ginseng Res.* **2002**, *26*, 151–158.
14. Lee, S.W.; Lee, S.H.; Park, K.H.; Lan, J.M.; Jang, I.B.; Kim, K.H. Inhibition effect on root rot disease of *Panax ginseng* by crop cultivation in soil occurring replant failure. *Korean J. Med. Crop Sci.* **2015**, *23*, 223–230. [CrossRef]
15. Jiao, X.L.; Zhang, X.S.; Lu, X.H.; Qin, R.; Bi, Y.M.; Gao, W.W. Effects of maize rotation on the physicochemical properties and microbial communities of American ginseng cultivated soil. *Sci. Rep.* **2019**, *9*, 8615. [CrossRef]
16. Bischoff Nunes, I.; Goodwin, P.H. Interaction of ginseng with *Ilyonectria* root rot pathogens. *Plants* **2022**, *11*, 2152. [CrossRef]
17. Westerveld, S.M.; Shi, F. 2021. The history, etiology, and management of ginseng replant disease: A Canadian perspective in review. *Can. J. Plant Sci.* **2021**, *101*, 886–901. [CrossRef]
18. He, C.N.; Gao, W.W.; Yang, J.X.; Bi, W.; Zhang, X.S.; Zhao, Y.J. Identification of autotoxic compounds from fibrous roots of *Panax quinquefolium* L. *Plant Soil* **2009**, *318*, 63–72. [CrossRef]
19. Yousef, L.F.; Bernards, M.A. In vitro metabolism of ginsenosides by the ginseng root pathogen *Pythium irregulare*. *Phytochemistry* **2006**, *67*, 1740–1749. [CrossRef]
20. OMAFRA. *Guide to Ginseng Production*; Queen's Printer for Ontario: Toronto, ON, Canada, 2015.
21. Kernaghan, G.; Reeleder, R.D.; Hoke, S.M.T. Quantification of *Cylindrocarpon destructans f.* sp. *panacis* in soils by real-time PCR. *Plant Pathol.* **2007**, *56*, 508–516.
22. Edgar, R.C. UPARSE: Highly accurate OTU sequences from microbial amplicon reads. *Nat. Methods* **2013**, *10*, 996–998. [CrossRef]
23. Callahan, B.J.; McMurdie, P.J.; Rosen, M.J.; Han, A.W.; Johnson, A.J.A.; Holmes, S.P. DADA2: High resolution sample inference from Illumina amplicon data. *Nat. Methods* **2016**, *13*, 581–583. [CrossRef] [PubMed]

24. Quast, C.; Pruesse, E.; Yilmaz, P.; Gerken, J.; Schweer, T.; Yarza, P.; Peplies, J.; Glöckner, F.O. The SILVA ribosomal RNA gene database project: Improved data processing and web-based tools. *Nucleic Acids Res.* **2013**, *41*, D590–D596. [CrossRef] [PubMed]

25. UNITE Community. *UNITE QIIME release for Fungi 2*; Version 18.11.2018; UNITE Community: Brisbane, QLD, Australia, 2019.

26. Edgar, R.C. MUSCLE: A multiple sequence alignment method with reduced time and space complexity. *BMC Bioinform.* **2004**, *5*, 113. [CrossRef] [PubMed]

27. Stamatakis, A. RAxML version 8: A tool of phylogenetics analysis and post-analysis of large phylogenies. *Bioinformatics* **2014**, *30*, 1312–1313. [CrossRef] [PubMed]

28. Kumar, S.; Stecher, G.; Tamura, K. MEGA7: Molecular evolutionary genetics analysis version 7.0 for bigger datasets. *Mol. Biol. Evol.* **2016**, *33*, 1870–1874. [CrossRef] [PubMed]

29. Langmead, B.; Salzberg, S.L. Fast gapped-read alignment with Bowtie2. *Nat. Methods* **2012**, *9*, 357–359. [CrossRef] [PubMed]

30. Li, B.; Dewey, C.N. RSEM: Accurate transcript quantification from RNA-Seq data with or without a reference genome. *BMC Bioinform.* **2011**, *12*, 323. [CrossRef] [PubMed]

31. Li, H.; Handsaker, B.; Wysoker, A.; Fennell, T.; Ruan, J.; Homer, N.; Marth, G.; Abecasis, G.; Durbin, R.; 1000 Genome Project Data Processing Subgroup. The Sequence Alignment/Map format and SAMtools. *Bioinformatics* **2009**, *25*, 2078–2079. [CrossRef]

32. Grabherr, M.G.; Haas, B.J.; Yassour, M.; Levin, J.Z.; Thompson, D.A.; Amit, I.; Adiconis, X.; Fan, L.; Raychowdhury, R.; Zeng, Q.; et al. Full-length transcriptome assembly from RNA-Seq data without a reference genome. *Nat. Biotechnol.* **2011**, *29*, 644–652. [CrossRef]

33. Robinson, M.D.; Oshlack, A. A scaling normalization method for differential expression analysis of RNA-seq data. *Genome Biol.* **2010**, *11*, R25. [CrossRef]

34. Robinson, M.D.; McCarthy, D.J.; Smyth, G.K. edgeR: A Bioconductor package for differential expression analysis of digital gene expression data. *Bioinformatics* **2010**, *26*, 139–140. [CrossRef] [PubMed]

35. Maechler, M.; Rousseeuw, P.; Struyf, A.; Hubert, M.; Hornik, K. *Cluster: Cluster Analysis Basics and Extensions*, R package version 2.1.0.; R Foundation for Statistical Computing: Vienna, Austria, 2019.

36. Ivanov, D.A.; Georgakopoulos, J.R.C.; Bernards, M.A. The chemoattractant potential of ginsenosides in the ginseng—*Pythium irregulare* pathosystem. *Phytochemistry* **2016**, *122*, 56–64. [CrossRef] [PubMed]

37. Kroetsch, D.B.H.; Wang, C. Particle size distribution. In *Soil Sampling and Methods of Analysis*, 2nd ed.; Carter, M.R., Gregorich, E.G., Eds.; Lewis Publishers: Boca Raton, FL, USA, 1993; pp. 499–511.

38. Zhang, Y.L.; Chen, J.B.; Lei, Y.; Zhou, Q.; Sun, S.Q.; Noda, I. Evaluation of different grades of ginseng using Fourier-transform infrared and two-dimensional infrared correlation spectroscopy. *J. Mol. Struct.* **2010**, *974*, 94–102. [CrossRef]

39. Isutsa, D.K.; Merwin, I.A. *Malus* germplasm varies in resistance or tolerance to apple replant disease in a mixture of New York orchard soils. *HortScience* **2000**, *35*, 262–268. [CrossRef]

40. Farh, M.E.A.; Kim, Y.J.; Kim, Y.J.; Yang, D.C. *Cylindrocarpon destructans/Ilyonectria radicicola*-species complex: Causative agent of ginseng root-rot disease and rusty symptoms. *J. Ginseng Res.* **2018**, *42*, 9–15. [CrossRef] [PubMed]

41. Shin, K.C.; Oh, D.K. Classification of glycosidases that hydrolyze the specific positions and types of sugar moieties in ginsenosides. *Crit. Rev. Biotechnol.* **2016**, *36*, 1036–1049. [CrossRef] [PubMed]

42. Wu, H.; Yang, H.; You, X.; Li, Y. Diversity of endophytic fungi from roots of *Panax ginseng* and their saponin yield capacities. *SpringerPlus* **2013**, *2*, 107. [CrossRef] [PubMed]

43. Court, W.A.; Reynolds, L.B.; Hendel, J.G. Influence of root age on the concentration of ginsenosides of American ginseng (*Panax quinquefolium*). *Can. J. Plant Sci.* **1996**, *76*, 853–855. [CrossRef]

44. Park, C.S.; Yoo, M.H.; Noh, K.H.; Oh, D.K. Biotransformation of ginsenosides by hydrolyzing the sugar moieties of ginsenosides using microbial glycosidases. *Appl. Microbiol. Biotechnol.* **2010**, *87*, 9–19. [CrossRef]

45. Luo, L.F.; Yang, L.; Yan, Z.X.; Jiang, B.B.; Li, S.; Huang, H.C.; Liu, Y.X.; Zhu, S.S.; Yang, M. Ginsenosides in root exudates of *Panax notoginseng* drive the change of soil microbiota through carbon source different utilization. *Plant Soil* **2020**, *455*, 139–153. [CrossRef]

46. Goodwin, P.H. The rhizosphere microbiome of ginseng. *Microorganisms* **2022**, *10*, 1152. [CrossRef] [PubMed]